Solvothermal synthesis of SrTiO$_3$ nanoparticles precisely controlled in surface crystal planes and their photocatalytic activity

Takeshi Kimijima*, Kiyoshi Kanie, Masafumi Nakaya, Atsushi Muramatsu

Institute of Multidisciplinary Research for Advanced Materials, Tohoku University, 2-1-1 Katahira, Aoba-ku, Sendai 980-8577, Japan

ARTICLE INFO

ABSTRACT

Strontium titanate (SrTiO$_3$) nanoparticles of cubes, spheres, and flake-type morphology were obtained by a solvothermal synthesis in H$_2$O/polyols mixed solution. Size of cubic particles bounded by {1 0 0} faces was controlled in the range from 24 to 43 nm by the adjustment of initial volume ratio in H$_2$O/diethylene glycol. Cubic particles exhibited high decomposition activity of organic compounds under ultraviolet irradiation. On the other hand, flake-type particles bounded mainly by {1 1 0} faces were obtained in H$_2$O/ethylene glycol solution system, highly active for H$_2$ evolution in photocatalytic reaction. These results indicate that the {1 0 0} surface shows high oxidative activity and that the {1 1 0} surface shows high reductive activity.

© 2013 Elsevier B.V. All rights reserved.

1. Introduction

Photocatalysts have attracted much attention because of their potentials in solving the energy and environmental problems by hydrogen production and/or decomposition of organic pollutant [1,2]. Strontium titanate (SrTiO$_3$) is very attractive material for photocatalyst because SrTiO$_3$ shows high photocatalytic activity under ultraviolet and visible light [3,4]. Generally speaking for heterogeneous catalysts, their activity is basically influenced by crystal phase, size, surface area, and crystallinity [5–8]. Nanoparticulate photocatalysts have advantages of large surface area and short diffusion distance of photo-excited electrons to the surface. Their morphology and outer surface also affect their photocatalytic activity. Namely, shape-controlled TiO$_2$ nanoparticles bounded by {0 0 1} faces have been reported to show high photocatalytic activity for H$_2$ evolution from aqueous ethanolic solution in our preceding study [9]. Some theoretical [10] and some experimental studies [9,11,12] also indicated that (0 0 1) surface of anatase-type TiO$_2$ shows high photocatalytic activity for hydrogen evolution because dissociative adsorption of water occur easier on the (0 0 1) surface than other faces. In this regard, the precise control in size and shape of SrTiO$_3$ is critically important so as to evaluate the face-dependent photoreactivity and develop high-performance photocatalyst. However, in spite of the previous extensive efforts, such a precise control in their size and shape has been fragmented and limited. A conventional synthesis of SrTiO$_3$ has been carried

out by solid state reaction at high temperature (800–1300 °C) for 10–20 h [12,13]. In this case, powders have been obtained with grinding it so that they are inhomogeneous in size and shape. Although chemical synthesis processes, such as sol–gel [14], oxalate [15], and combustion methods [16] have also been reported, they are also required to calcine at high temperature so as to crystallize. Such a method cannot satisfy the precise control in particle size and shape. Recently, nanoparticles were synthesized in liquid phase reaction [17–21]. Our previous study also developed the liquid phase synthesis of about 40 nm-sized SrTiO$_3$ particles [22]. However, morphology control has not been adequately achieved yet.

In the present study, the precise control in morphology of SrTiO$_3$ nanoparticles has been established in H$_2$O/polyols mixed solution. The evaluation of photocatalytic activities of cubic, spherical, and flake-type particles will be well compared so that the highest crystal facet can be identified.

2. Experimental

2.1. Preparation of SrTiO$_3$ nanoparticles

Titanium tetraisopropoxide (TIPO) was mixed with triethanolamine (TEOA) under a dry atmosphere at room temperature for 1 day in order to form stable titanium–triethanolamine (Ti–TEOA) complex against the hydrolysis by water [23]. The solvent, such as an ion-exchange water, ethylene glycol (EG), diethylene glycol (DEG), or trimethylene glycol (TMG), was added to Ti–TEOA complex to fill up the determined volume. Here, the molar ratio of TEOA/TIPO was adjusted to 2/1 and the Ti^{4+} concentration to 0.50 M. Then, 10 mL of H$_2$O and/or polyol

* Corresponding author. Tel.: +81 22 217 5164; fax: +81 22 217 5165.
E-mail address: kimijima@mail.tagen.tohoku.ac.jp (T. Kimijima).

were poured into the 10 mL of the Ti–TEOA complex solution in the reaction vessel. At this point, the volume ratio of H_2O/polyol was varied from 100/0 to 0/100. Next, $Sr(OH)_2$ $8H_2O$ (1.32 g, 5.0 mmol) was added to the solution under stirring. The resulting mixture became white-colored gel after 90 min at room temperature. The gel was placed into a 23 mL Teflon-lined autoclave and aged at 140 °C for 72 h. Precipitates formed by the aging were collected by centrifugation (18,000 rpm, 10 min) and washed three times with ion-exchange water. As a comparison, $SrTiO_3$ powder (**S-ST**) was prepared by a conventional solid state reaction as follows [24]. Stoichiometric amount of TiO_2 (99.9%, Wako Chemical) and $SrCO_3$ (99.9% Wako Chemical) were mixed well and then calcined at 1000 °C for 10 h in air.

2.2. Characterization

Crystal structures were characterized by X-ray diffractometry (XRD) with a Rigaku UltimaIV system equipped with a Cu Kα source at 40 kV and 40 mA. Relative XRD peak area ratio of $SrTiO_3$ (1 1 0) peak and rutile-type TiO_2 (1 1 0) peak, which was defined as relative crystallinity (R_C), was measured after mixing 67 wt.% of as-prepared $SrTiO_3$ and 33 wt.% of well-crystalline rutile-type TiO_2 (99.0%, Wako Chemical) as an inside standard. The particle morphology was observed by a Hitachi H-7650 transmission electron microscopy (TEM) at 100 kV. The particle mean sizes and the standard deviation of $SrTiO_3$ particles were calculated by counting 100 particles taken by the TEM. Electron diffraction (ED) measurement and high-resolution TEM (HRTEM) images obtained by a JEOL JEM-3010 system at 300 kV, were performed to determine crystal orientation. Elemental analysis was carried out by X-ray fluorescence analysis (XRF, Rigaku ZSX PrimusII). The surface area of the $SrTiO_3$ nanoparticles were determined by Brunauer–Emmett–Teller (BET) measurements with a BELSORP-mini purchased from BEL Company. The quantitative analysis of evolved gases was carried out by gas chromatography with thermal conductivity detector with a Shimadzu GC-8A.

2.3. Photocatalytic activity test of $SrTiO_3$ nanoparticles

Photocatalytic activity of size- and shape-controlled $SrTiO_3$ nanoparticles obtained in the present study was evaluated as follows. The amount of H_2 evolution from methanolic aqueous solution and decomposition of acetic acid in water was measured as a photocatalytic activity. Initially, as-prepared $SrTiO_3$ nanoparticles (100 mg) and hexachloroplatinic acid ($H_2PtCl_6 \cdot 6H_2O$) were dispersed or dissolved in 10 mL of 50 vol.% methanolic aqueous solution in a rubber septum-capped Pyrex bottle. The loading amount of Pt was adjusted to 0.50 wt.%. After the mixture was bubbled well with Ar gas, the photo-irradiation to the bottle was carried out with a 500 W high-pressure mercury lamp (Wacom BMO-500DJ) without any filter under vigorous stirring. Finally, the quantities of evolved gases were determined by gas chromatog-
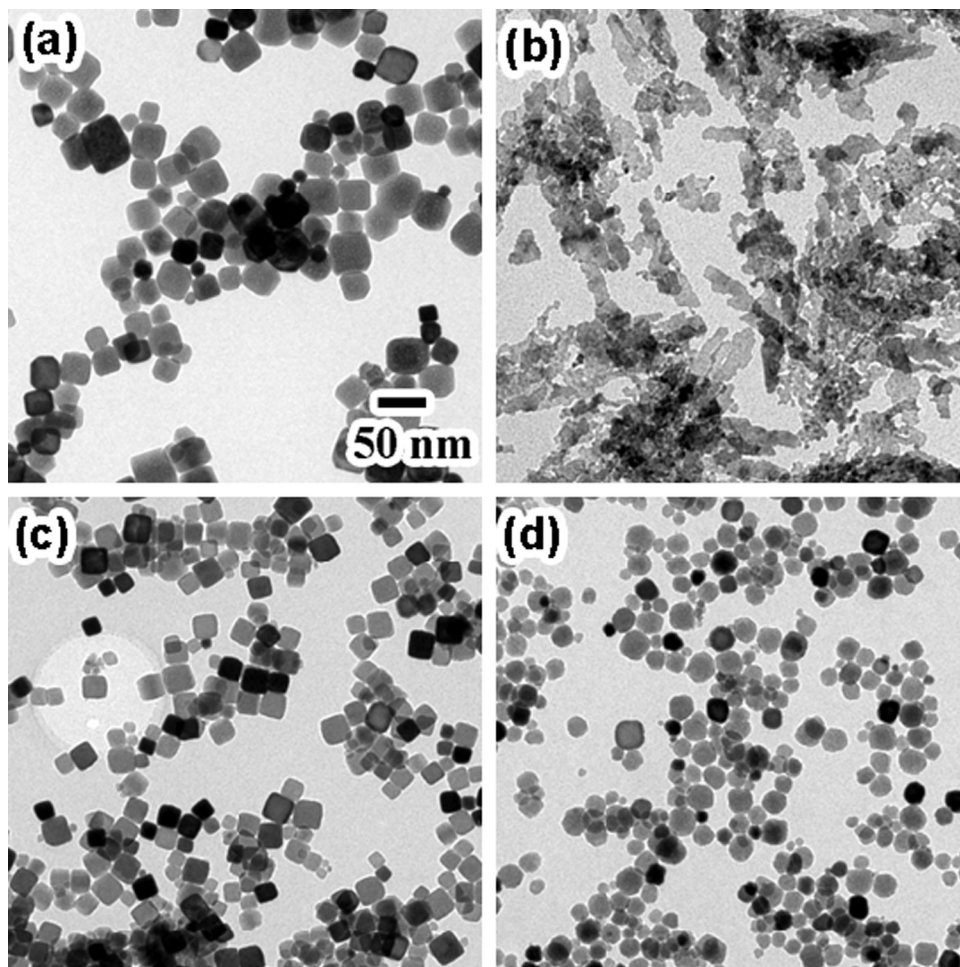

Fig. 1. TEM images of $SrTiO_3$ nanoparticles obtained in H_2O/polyols mixed solutions: (a) H_2O: **ST1**; (b) H_2O/EG: **ST2**; (c) H_2O/DEG: **ST3** and (d) H_2O/TMG: **ST4**. The volume ratio of H_2O/organic solvents for (b–d) was fixed to 43/57 (v/v). The scale bar in (a) is common for all images.
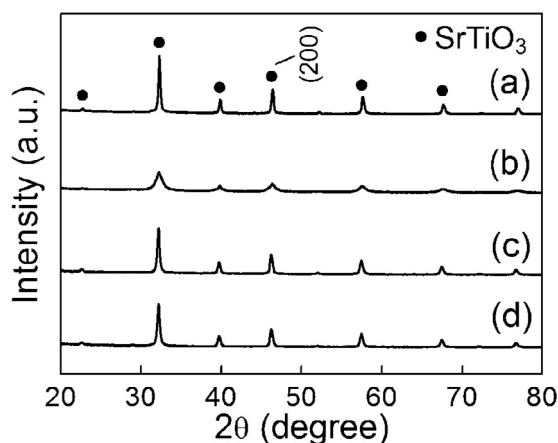
Fig. 2. XRD patterns of SrTiO$_3$ nanoparticles **ST1–4** prepared in H$_2$O/polyols mixed solution systems: (a) **ST1**: H$_2$O; (b) **ST2**: H$_2$O/EG; (c) **ST3**: H$_2$O/DEG and (d) **ST4**: H$_2$O/TMG. The volume ratio of H$_2$O/polyols for (b–d) was 43/57 (v/v).

raphy. Here, H$_2$ evolution rate was defined at the steady state. In the case of decomposition of acetic acid, reaction condition was almost the same as H$_2$ evolution case. The reaction was carried out in 5.0 vol.% acetic acid aqueous solution without co-catalyst under an air atmosphere. Then, evolved CO$_2$ was detected by gas chromatography.

3. Results and discussion

3.1. Solvothermal synthesis of SrTiO$_3$ nanoparticles in H$_2$O/polyols mixed solutions

Fig. 1 shows TEM images of precipitates obtained in solvent mixture of H$_2$O, H$_2$O/EG, H$_2$O/DEG, and H$_2$O/TMG, where the volume ratio of the H$_2$O/polyols was fixed to 43/57. As shown in Fig. 1, nanocubes with sharp edges were obtained in H$_2$O (denoted as **ST1**) and H$_2$O/DEG (**ST3**) systems, in contrast to the formation of nanoflakes in H$_2$O/EG (**ST2** Fig. 1b) and nanospheres in H$_2$O/TMG (**ST4**). As a result, the particle morphology was readily controlled by choice of the polyols used as a solvent. The particle mean sizes and the standard deviation of **ST1**, **ST3**, and **ST4** were 43.0 ± 10.5, 30.4 ± 6.5, and 28.0 ± 6.5 nm, respectively. Crystal structure of as-prepared **ST1–4** was confirmed by XRD analysis. As shown in Fig. 2, a cubic SrTiO$_3$ phase (JCPDS No. 035-0734) is successfully obtained in a single phase for all cases. The crystallite sizes of **ST1**, **ST2**, **ST3**, and **ST4** were calculated as 43.9, 15.5, 33.5, and 28.9 nm, respectively, from (2 0 0) peak of the XRD patterns with Scherrer's equation. Since the particle mean sizes of **ST1**, **ST3**, and **ST4** were almost the same as the crystallite sizes, nanocubes, **ST1** and **ST3**, and nanospheres **ST4** must be single crystalline. The Sr/Ti molar ratios of **ST1**, **ST2**, **ST3**, and **ST4**, were confirmed as 0.98, 0.95, 1.0, and 0.99, respectively, from XRF analysis, so that almost all the particles in **ST1–4** were formed purely in structure.
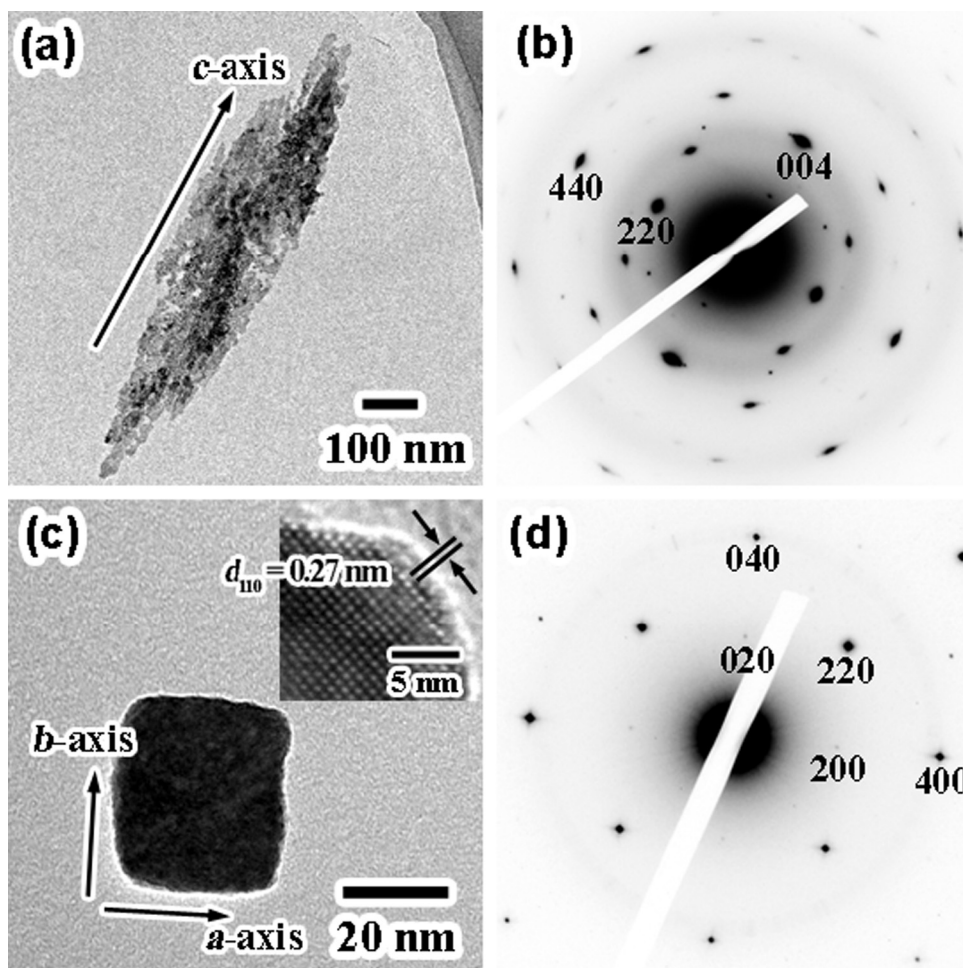

Fig. 3. HRTEM images of (a) **ST2** and (c) **ST3** shown in Fig. 1b and c, respectively, and their ED patterns of (b) **ST2** and (d) **ST3**.

HRTEM images and their ED pattern of **ST2** and **ST3** are exhibited in Fig. 3. ED spots assigned as (0 0 4) and (0 0 −4) planes of **ST2** were observed toward parallel to the growing direction of flake-type particle. This morphology is controlled through anisotropic growth along *c*-axis, possibly because of the specific adsorption of EG on planes parallel to *c*-axis. As a result, **ST2** is bounded by {1 1 0} faces. On the other hand, the lattice spacing of **ST3** was determined as 0.27 nm by HRTEM images (Fig. 3c), in consistent with the spacing of {1 1 0} planes of $SrTiO_3$ at 0.27590 nm (JCPDS No 035-0734). The ED spots can be indexed as the [0 0 1] zone axis (Fig. 3d). Namely, the **ST3** particle is bounded by {1 0 0} faces. The shape control of **ST3** to nanocube must be due to adsorption of TEOA specifically on to the {1 0 0} planes so that the crystal growth is inhibited along ⟨1 0 0⟩ direction. However, TEOA adsorption uptake was weakened when TMG was introduced as a solvent so that different shaped particles, nanospheres, were formed (Fig. 1d), possibly because of TMG inhibition against the specific adsorption of TEOA. Both of the specific adsorption of TEOA and solvent effect of glycols is the competitive factor for the control of final particle shape, such as, cube, flake-type, and sphere [25].

3.2. Effect of H_2O/EG, DEG or TMG mixing ratio on their size and shape

As the solvent effect of EG was found considerable, the effect of H_2O/EG ratio on the morphology and size was investigated. Judging from TEM images of particles obtained with different H_2O/EG volume ratios ((a) $H_2O/EG = 86/14$; (b) 72/28; (c) 59/41; (d) 8/92) in Fig. 4 drastic morphological change was observed. Nanospheres are obtained when the EG ratios are 14–28 vol.% (Fig. 4a and b). Snbmicron-sized spherical particles (100–150 nm) are synthesized at $H_2O/EG = 59/41$ (Fig. 4c). Nanoflakes were formed in H_2O/EG mixtures from 43/57 vol.% to 8/92 vol.% (Figs. 1b and 4d). The XRD measurement of the particles confirmed formation of $SrTiO_3$ in a single phase until 92 vol.%. Impurity phases, such as SrO and TiO_2 were observed at $H_2O/EG = 2/98$.

Also, effect of H_2O/DEG ratio was considerable so that Fig. 5 shows the TEM images of particles prepared at different H_2O/DEG volume ratios ((a) $H_2O/DEG = 86/14$; (b) 59/41; (c) 45/55; (d) 28/72). In all cases, particle was shaped as a cube with sharp edge. The particle mean size and the standard deviation are calculated as 40.5 ± 11.1, 30.4 ± 7.2, 28.0 ± 6.5, and 23.9 ± 4.2 nm from Fig. 5a–d, respectively. Namely, the particle size was decreased from 43 to 24 nm by increase in DEG volume ratio in H_2O/DEG mixtures from 0 vol.% to 72 vol.%. Further increase in DEG up to 78 vol.% resulted in the formation of irregular-shaped $SrTiO_3$ nanoparticles of ca. 15 nm. This decrease in H_2O led to the reduction of the solubility of direct precursors of the particles so that the nucleation may continue in the particle growth step. Such a effect was also observed in H_2O/TMG systems.
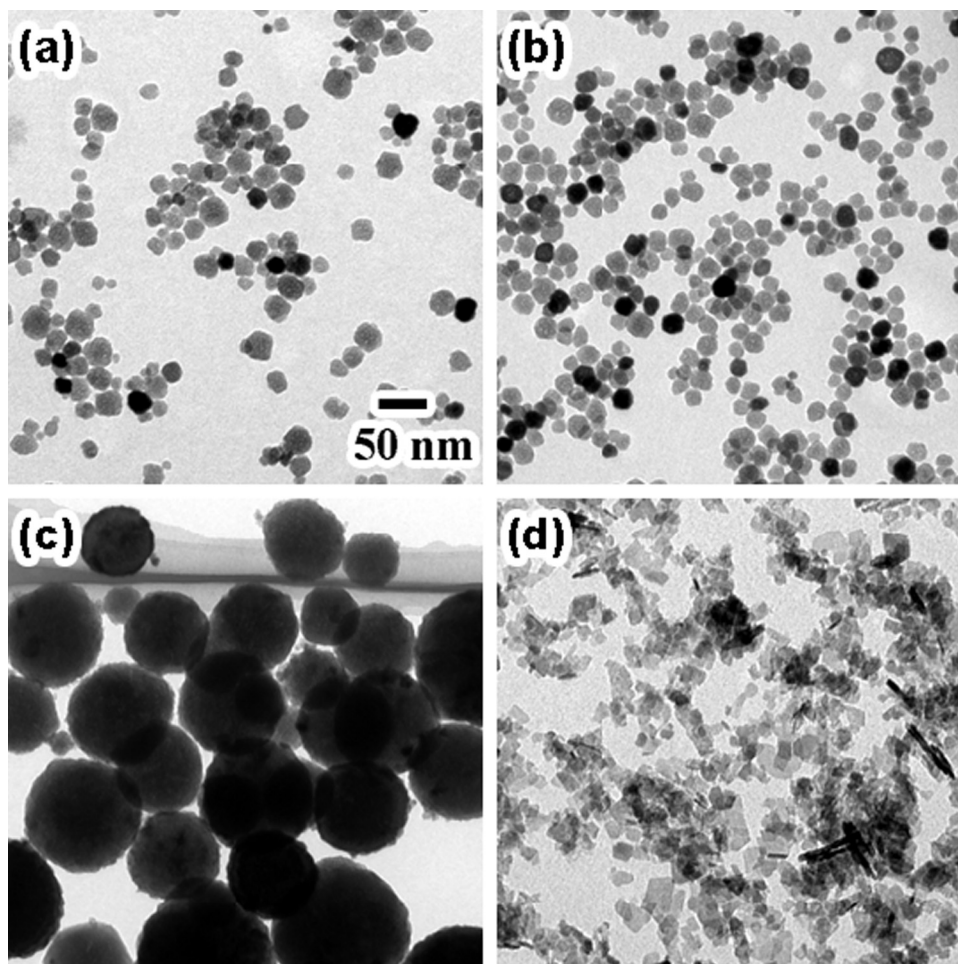

Fig. 4. TEM images of $SrTiO_3$ nanoparticles synthesized by changing initial H_2O/EG volume ratios: the volume ratios of H_2O/EG were adjusted to (a) 86/14, (b) 72/28, (c) 59/41, and (d) 8/92 (v/v).
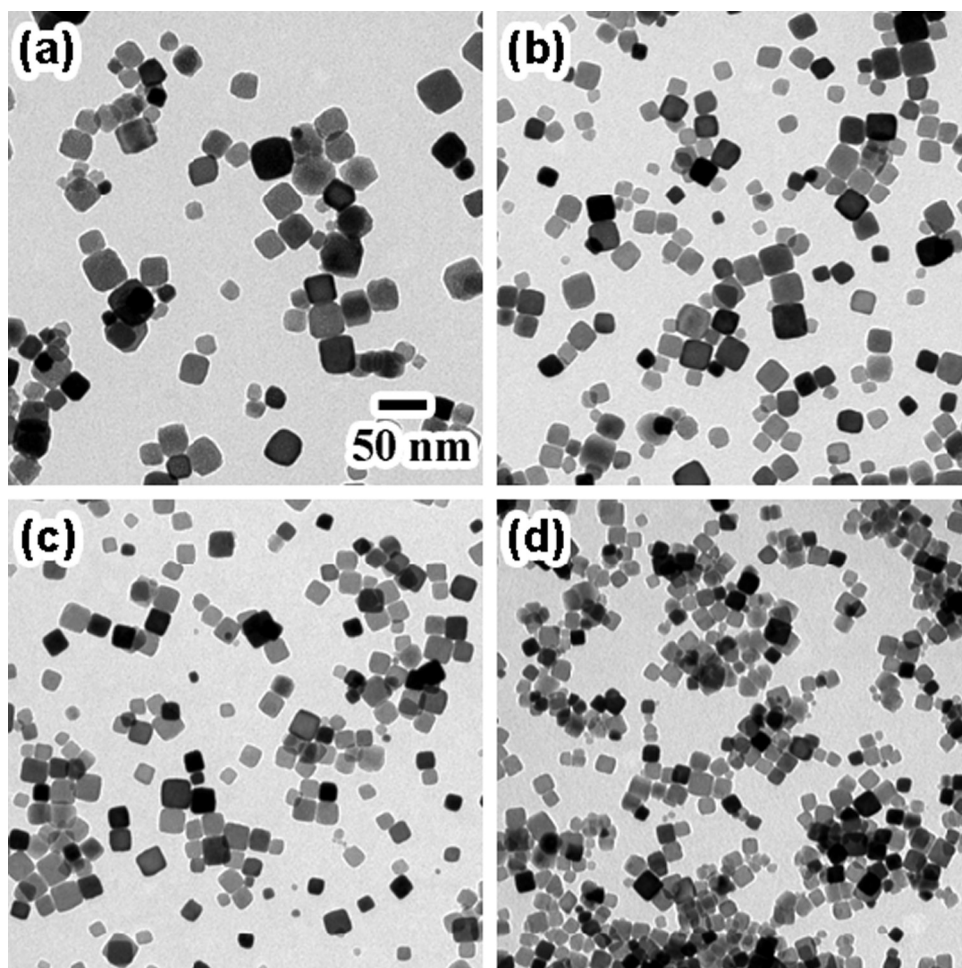
Fig. 5. TEM images of $SrTiO_3$ nanoparticles synthesized by controlling the H_2O/DEG mixing ratios: The volume ratios of H_2O/DEG were (a) 86/14; (b) 59/41; (c) 45/55 and (d) 28/72 (v/v).

3.3. Photocatalytic activity of $SrTiO_3$ nanoparticles with nanoflakes, nanocubes, and nanospheres

H_2 and CO_2 evolution from photo-decomposition of methanol and acetic acid on **ST1**–**4** and **S-ST** are illustrated in Figs. 6 and 7, respectively. The specific surface area, relative crystallinity (R_C), and H_2 and CO_2 evolution rates will also be summarized in Table 1. Highest surface area was found for nanoflakes (**ST2**) because of their remarkable surface roughness, in contrast to the other particles.

In addition, **ST2** showed the lowest relative crystallinity, possibly because of the polycrystal-like structures judging from TEM observation. The specific surface area of the finer nanocubes (**ST3**) was ca. twice the larger than **ST1**. **ST2** showed highest H_2 evolution among samples tested. In spite of the similar shape but difference in size, **ST3** exhibits almost same activity as **ST1**. To support this result, the H_2 evolution rates of cubic-shaped particles obtained at various H_2O/DEG ratios, exhibited in Fig. 5, were also measured (Fig. 8). These particles showed similar catalytic activities regardless of the
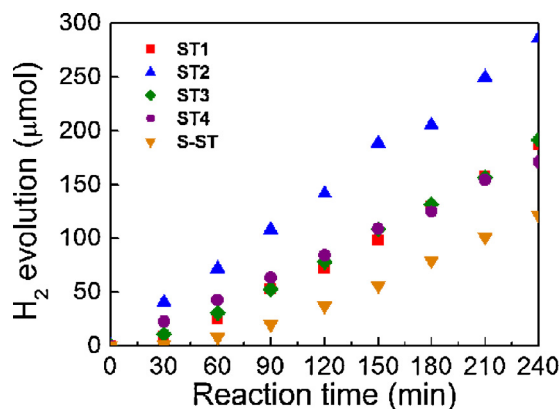

Fig. 6. Photocatalytic activity for H_2 evolution of the solvothermally prepared $SrTiO_3$ nanoparticles **ST1**–**4** and **S-ST** obtained by solid phase synthesis.
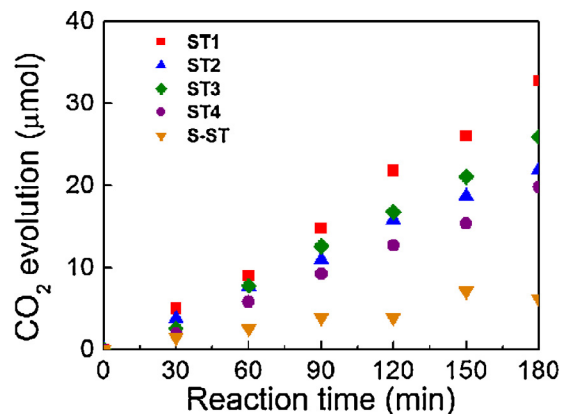

Fig. 7. Photocatalytic activity for CO_2 evolution of the solvothermally prepared $SrTiO_3$ nanoparticles **ST1**–**4** and **S-ST** obtained by solid phase synthesis.

Table 1
Specific surface area, relative crystallinity R_C (SrTiO$_3$/TiO$_2$), and H$_2$ and CO$_2$ evolution rate of **ST1**–**4**, and **S-ST**.

	Specific surface area (m^2 g^{-1})	R_C[a]	H$_2$ (μmol h^{-1})[b]	CO$_2$ (μmol h^{-1})[b]
ST1	24.2	3.00	53.3	11.3
ST2	120	2.24	69.6	7.66
ST3	43.2	3.21	51.3	9.16
ST4	49.7	2.90	42.3	6.96
S-ST	9.31	4.00	42.3	2.29

[a] Relative crystallinity, which was evaluated by the comparison of the XRD peak area ratio of synthesized SrTiO$_3$ {1 1 0} peak with commercial TiO$_2$ rutile {1 1 0} peak.
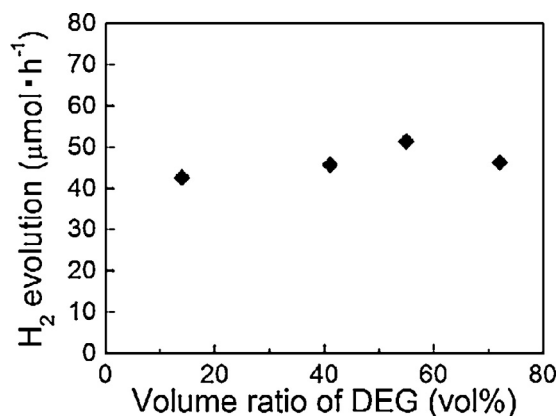
[b] Gas evolution rate at steady state.

Fig. 8. Hydrogen evolution rate of the cubic-shaped SrTiO$_3$ nanoparticles obtained at various H$_2$O/DEG ratios. The TEM images of the particles are shown in Fig. 5.

values of the specific surface area. Therefore, the specific surface area and crystallinity seems not a critical factor for the H$_2$ evolution activity, but the surface plane is remarkably considerable for the photocatalyst design. As has been reported already, {0 0 1} surface of TiO$_2$, shows higher activity than other faces [3,8]. In this regard, the highest photocatalytic activity of **ST2** must be due to {1 1 0} as their outer surfaces. On the other hand, the largest yield of CO$_2$ was recorded on **ST1** and the second **ST3**, as both is nanocubes with {1 0 0} facet. The activity difference between {1 1 0} and {1 0 0} surface due to the difference of reductive and oxidative site density on these surface [26,27]. Photoexcited electron might be more likely to move on {1 1 0} surface. Since H$_2$ production from methanol as a sacrifice reagent is considered as the rate-determining step, [28] the water splitting to give H$_2$ is expected to selectively occur on {1 1 0} surfaces. On the other hand, oxidative reaction tends to take place on {1 0 0} faces.

4. Conclusion

SrTiO$_3$ nanoparticles of different shape, that is, cube, sphere, and flake-like, were prepared by a solvothermal method in H$_2$O,

H$_2$O/EG, H$_2$O/DEG, and H$_2$O/TMG mixed solvents. The size of nanocubes and nanospheres were controlled by the H$_2$O/DEG and H$_2$O/TMG ratios. The particle size was decreased from 43 to 24 nm with an increase in H$_2$O/DEG ratio from 0 vol.% to 72 vol.%. Nanoflakes bounded by {1 1 0} surface showed higher photocatalytic activity than other particles for H$_2$ evolution. On the other hand, nanocubes by {1 0 0} surface exhibited higher photocatalytic activity for decomposition of acetic acid in water. Since photoexcited electron may tend to be trapped selectively on {1 1 0} surface, {1 1 0} faces showed high activity for H$_2$ evolution reaction, accounting for the surface structure effect to the catalytic activities.

References

[1] A. Kudo, Y. Miseki, Chemical Society Reviews 38 (2009) 253–278.
[2] M. Sturini, A. Speltini, F. Maraschi, A. Profumo, L. Pretali, E.A. Irastorza, E. Fasani, A. Albini, Applied Catalysis B: Environmental 119–120 (2012) 32–39.
[3] K. Domen, A. Kudo, T. Onishi, N. Kosugi, H. Kuroda, Journal of Physical Chemistry 90 (1986) 292–295.
[4] R. Konta, T. Ishii, H. Kato, A. Kudo, Journal of Physical Chemistry B 108 (2004) 8992–8995.
[5] H.G. Yang, G. Liu, S.Z. Qiao, C.H. Sun, Y.G. Jin, S.C. Smith, J. Zou, H.M. Cheng, G.Q. Lu, Journal of the American Chemical Society 131 (2009) 4078–4083.
[6] M.L. Scullin, J. Ravichandran, C. Yu, M. Huijben, J. Seidel, A. Majumdar, R. Ramesh, Acta Materialia 58 (2010) 457–463.
[7] J.A. Enterkin, K.R. Poeppelmeier, L.D. Marks, Nano Letters 11 (2011) 993–997.
[8] Z. Liu, T. Yamazaki, Y. Shen, D. Meng, T. Kikuta, N. Nakatani, Chemistry Letters 37 (2008) 296–297.
[9] T. Kimijima, T. Sasaki, M. Nakaya, K. Kanie, A. Muramatsu, Chemistry Letters 39 (2010) 1080–1081.
[10] X.-Q. Gong, A. Selloni, Journal of Physical Chemistry B 109 (2005) 19560–19562.
[11] F. Amano, T. Yasumoto, O.-O. Prieto-Mahaney, S. Uchida, T. Shibayama, B. Ohtani, Chemical Communications (2009) 2311–2313.
[12] F. Amano, O.-O. Prieto-Mahaney, Y. Terada, T. Yasumoto, T. Shibayama, B. Ohtani, Chemistry of Materials 21 (2009) 2601–2603.
[13] S.W. Bae, P.H. Borse, J.S. Lee, Applied Physics Letters 92 (2008) 104107.
[14] V. Somani, S.J. Kalita, Journal of Electroceramics 18 (2007) 57–65.
[15] Y.S. Malghe, Journal of Thermal Analysis and Calorimetry 102 (2010) 831–836.
[16] S. Liu, Z. Xiu, J. Liu, F. Xu, W. Yu, J. Yu, G. Feng, Journal of Alloys and Compounds 457 (2008) L12–L14.
[17] T. Tsumura, K. Matsuoka, M. Toyoda, Journal of Materials Science and Technology 26 (2010) 33–38.
[18] M. Niederberger, G. Gamweitner, N. Pinna, M. Antonietti, Journal of the American Chemical Society 126 (2004) 9120–9126.
[19] M. Makarova, A. Dejneka, J. Franc, J. Drahokoupil, L. Jastrabik, V. Trepakov, Optical Materials 32 (2010) 803–806.
[20] S. Fuentes, R.A. Zarate, E. Chavez, P. Munoz, D. Diaz-Droguett, P. Leyton, Journal of Materials Science 45 (2010) 1448–1452.
[21] Q. Liu, Z. Yan, G. Sun, W. Zheng, Chemistry Letters 36 (2007) 458–459.
[22] J. Cuya, N. Sato, K. Yamamoto, H. Takahiashi, A. Muramatsu, Thermochimica Acta 419 (2004) 215–221.
[23] T. Sugimoto, X. Zhou, A. Muramatsu, Journal of Colloid and Interface Science 259 (2003) 53–61.
[24] Y. Sasaki, H. Nemoto, K. Saito, A. Kudo, Journal of Physical Chemistry C 113 (2009) 17536–17542.
[25] X. Jiang, Y. Wang, T. Herricks, Y. Xia, Journal of Materials Chemistry 14 (2004) 695–703.
[26] T. Ohno, K. Sarukawa, M. Matsumura, New Journal of Chemistry 26 (2002) 1167–1170.
[27] T. Tachikawa, S. Yamashita, T. Majima, Journal of the American Chemical Society 133 (2011) 7197–7204.
[28] K. Maeda, K. Teramura, H. Masuda, T. Takata, N. Saito, Y. Inoue, K. Domen, Journal of Physical Chemistry B 110 (2006) 13107–13112.